6.7-nm Emission from Gd and Tb Plasmas over a Broad Range of Irradiation Parameters Using a Single Laser

Liang Yin,[1,2,*] Hanchen Wang,[2,3] Brendan A. Reagan,[1,2] Cory Baumgarten,[1,3] Eric Gullikson,[4] Mark Berrill,[2,5] Vyacheslav N. Shlyaptsev,[1,2] and Jorge J. Rocca[1,2,3]

[1]*Engineering Research Center for Extreme Ultraviolet Science and Technology, Colorado State University, Fort Collins, Colorado 80523, USA*

[2]*Department of Electrical and Computer Engineering, Colorado State University, Fort Collins, Colorado 80523, USA*

[3]*Department of Physics, Colorado State University, Fort Collins, Colorado 80523, USA*

[4]*Center for X-Ray Optics, Lawrence Berkeley National Laboratory, Berkeley, California 94720-8199, USA*

[5]*Oak Ridge National Laboratory, Oak Ridge, Tennessee 37831, USA*

(Received 29 March 2016; revised manuscript received 13 July 2016; published 15 September 2016)

We report a comprehensive study of the emission from Gd and Tb laser-produced plasmas in the 6.5–6.7-nm wavelength region for a broad range of laser-irradiation parameters using a single $\lambda = 1030$ nm laser with tunable pulse duration in the 120-ps-to-4-ns range. The results are of interest for beyond-extreme-ultraviolet (BEUV) lithography of integrated circuits. BEUV emission spectra are measured as a function of laser-pulse duration, emission angle, and spatial location within the plasma. Images of the BEUV-emitting plasma region at the BEUV wavelength are obtained as a function of irradiation parameters. The emission spectrum is observed to broaden and to shift to a longer wavelength as the duration of the driver laser pulses is shortened from nanoseconds to hundreds of picoseconds. Transient self-consistent hydrodynamic and atomic physics simulations show that the picosecond irradiation creates significantly hotter plasmas in which the dominant emission originates from more highly ionized species. Gd-plasma emission driven by nanosecond laser pulses spectrally best matches the responsivity of the energy monitors used, centered near $\lambda = 6.74$ nm. Spatially resolved spectra of the Gd plasma are acquired for different laser-pulse durations. The conversion efficiency (CE) of Gd/Tb plasma into a 0.6% bandwidth in a 2π solid angle is determined by integrating angularly resolved measurements obtained using an array of calibrated energy monitors. Similar maximum CEs of about 0.47% for both the Gd and Tb plasmas are obtained. The source size is measured to approximately match the spot size of the laser on target, in agreement with simulations.

DOI: 10.1103/PhysRevApplied.6.034009

I. INTRODUCTION

The continuous increase in the number of transistors per chip that has fueled the growth of the semiconductor industry for the past several decades [1] requires printing increasingly smaller features. Progress in lithography is key in enabling this growth. To make this possible, projection lithography using progressively shorter wavelengths has been employed in combination with other solutions. Immersion lithography with $\lambda = 193$ nm light and its combination with multiple patterning has been used for the past several years to continue reducing the critical dimension. This has allowed the semiconductor industry to reach the 14-nm node for MPU and DRAM as outlined in the International Technology Roadmap for Semiconductors in high-volume production using this wavelength, a remarkable achievement. However, the use of 193-nm illumination is approaching its ultimate limit [2]. Extreme-ultraviolet lithography (EUVL) using $\lambda = 13.5$ nm light generated from laser-produced Sn plasmas is being used by device manufacturers to develop processes for insertion into high-volume manufacturing at the 7-nm logic node. [3]. This technology, which has been in development for decades, will serve to manufacture the next generations of computer processors and other integrated circuits. Given the long time necessary to translate such complex technology into high-volume manufacturing, interest has recently arisen in light sources near $\lambda = 6.7$ nm for the development of the next-generation lithography, termed "beyond-extreme-ultraviolet lithography" (BEUVL), because of the availability of highly reflective mirrors at this wavelength.

Highly ionized Gd and Tb plasmas emitting at wavelengths near $\lambda = 6.7$ nm [4,5] in the form of an unresolved transition array are primary light-source candidates for BEUVL [6]. They can produce intense emission within the

*Corresponding author.
liangyin@rams.colostate.edu

reflection region of La/B-based multilayer mirrors, whose near-normal incidence reflectivity can theoretically reach values up to 80% [7]. A reflectivity of 64.1% at $\lambda = 6.65$ nm with a 0.06-nm FWHM bandwidth has been already realized experimentally [8]. Complementing research on high-reflectivity mirror coatings and photoresist, the development of a high-power light source at this wavelength is a significant challenge that must be addressed. The spectral profile of the emission is determined by the plasma parameters, in particular the ion-species distribution. The $n = 4$–4 transitions from Gd^{16+}–Gd^{20+} emit in the neighborhood of 6.7 nm [5]. Previously reported steady-state plasma computations have estimated that Gd plasmas have the maximum emission near 6.7 nm when the electron temperature T_e is around 120 eV [9]. The electron temperature is mainly determined by the laser intensity. Aside from the plasma temperature and density, the plasma size also plays a role in the emission, affecting both its rate of expansion and opacity. The rate of expansion determines the rate of adiabatic cooling [10] that affects the conversion efficiency of laser energy into BEUV emission.

The results of several previous studies of the emission from laser-produced Gd plasmas in the spectral region of interest for BEUVL have been published [4,9,11–15]. Measurements of CE as a function of laser intensity have been reported from different experiments conducted using different laser-pulse durations. In one of them, $\lambda = 1064$ nm wavelength pulses of 10-ns duration were used to achieve a CE of up to 0.3% into a 0.6% bandwidth in 2π solid angle and a maximum CE of 0.4% was reported using $\lambda = 1064$ μm 150-ps pulses from a different laser [11]. By using low density target and dual laser-pulse irradiation, the CE was observed to be as high as 0.54% when a main pulse intensity of 5.6×10^{12} W/cm^2 was used [12]. Another work reported a CE of 0.8% into the same bandwidth from one-dimensional spherical plasmas produced by a twelve-joule Nd: glass laser [13]. Laser pulses from a $\lambda = 10.6$ μm CO_2 laser have been reported to produce a maximum CE of 0.7% at a laser-irradiation intensity of 1.2×10^{11} W/cm^2 [14]. In all cases the CE results were obtained by measuring the 6.7-nm light emitted using a single detector placed at a fixed angle with respect to the target and assuming that the emission was isotropic. Other experiments have been conducted to observe the spectral distribution of the emission of interest [4,9,11–15], and one experiment reported the Gd-plasma-size plasma images obtained with an x-ray pinhole camera [13]. In summary, a significant amount of information has recently been obtained from different experiments conducted using different lasers.

In this paper, we report the results of a comprehensive study of the $\lambda = 6.7$ nm BEUV emission from laser-produced Gd and Tb plasmas over a broad range of irradiation pulse parameters using the same experimental setup and a single laser with pulse duration tunable from 120 ps to 4 ns for all the measurements. This allows for direct comparison of the results without the possible inconsistencies that could arise from comparisons of measurements made using different setups. A suite of diagnostics is employed including an array of five calibrated energy monitors that measure the angular distribution of the BEUV emission for angles ranging from normal incidence to grazing. This allows us to make more accurate estimates of the CE without assuming isotropic emission as in past measurements [11,13]. BEUV emission spectra are measured as a function of laser-pulse duration, emission angle, and spatial location within the plasma to understand the plasma conditions relevant to conversion efficiency. Images of the BEUV-emitting plasma region at BEUV wavelength are obtained as a function of irradiation parameters. CE and spectral measurements are also reported for Tb plasmas. A maximum CE of 0.47% into a 0.6% bandwidth centered at $\lambda = 6.74$ nm in a 2π solid angle is measured for a Gd plasma created by 2-ns laser pulses, and a similar CE of 0.45% is measured for a Tb plasma. The plasma physics behind the measured trends is discussed below with the support of transient hydrodynamic and atomic-physics simulations. The simulations are conducted using an upgraded version of the hydrodynamic and atomic-physics code RADEX [16–21], originally developed to simulate plasmas for soft x-ray laser amplification, employing a Lagrangian grid and atomic collisional and radiative rates from the HULLAC code [22]. RADEX calculates self-consistent radiation transport for several hundred thousand lines originating from more than 5000 levels of all possible ion stages. Radiation transport is computed using the Biberman-Holstein approximation.

II. EXPERIMENTAL SETUP

Figure 1 shows a schematic of the experiment setup. We use a diode-pumped, chirped-pulse amplification laser system based on a cryogenically cooled Yb:YAG (where YAG is yttrium aluminum garnet) amplifier that produces pulses with energies of up to 100 mJ at $\lambda = 1030$ nm [23,24]. This laser provides pulses with a duration ranging from 120 ps to 4 ns at a repetition rate of up to 100 Hz. Its output can also be boosted up to 1 J installing an additional amplifier [25,26], but the experiments reported here are conducted at energies below 100 mJ. Laser pulses of 120–220-ps durations are generated by adjusting the grating pulse stretcher. Durations of 2–4 ns are produced by operating the regenerative amplifier in Q-switched cavity dumped mode and subsequently temporally clipping the pulses to the desired pulse duration using a Pockels cell and a polarizer pair prior to further amplification. This approach preserves the laser-beam spatial characteristics when the laser is switched between different pulse durations, allowing for a more direct comparison of the dependence of BEUV emission on pulse duration than if different lasers are used. Pulses from this laser are focused in vacuum onto

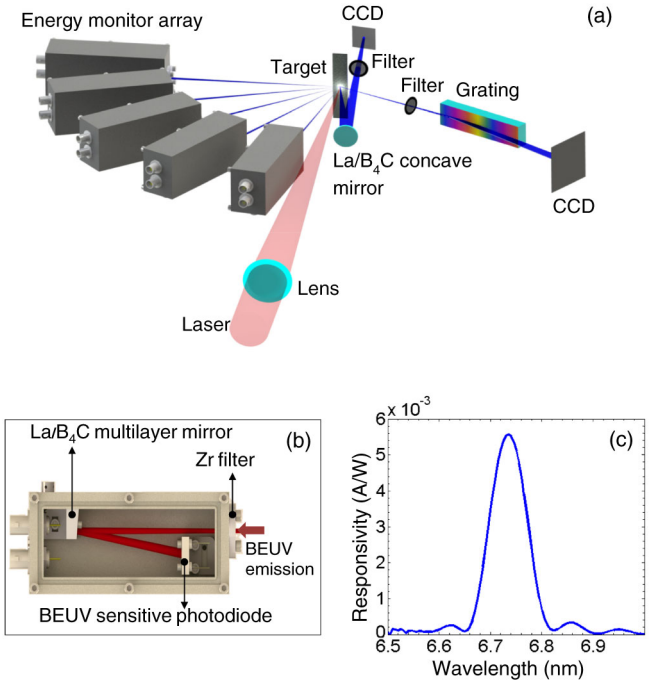

FIG. 1. (a) Schematic diagram of the experiment setup. (b) Internal configuration of the energy monitors. (c) Absolute calibration of the responsivity of one of the energy monitors measured using the ALS synchrotron.

polished Gd and Tb slab targets using three different lenses to obtain focal spot diameters of 30, 55, and 85-μm FWHM. The targets are mounted on a motorized stage in order to renew the target surface after each shot. Consequently, the average BEUV output power is expected to increase linearly as a function of repetition rate, provided absorption of the generated radiation by an increased amount of vapor in the chamber is not an issue.

An array of five calibrated BEUV energy monitors is used to simultaneously measure the angular distribution of the BEUV emission on every shot. These energy monitors are positioned on an 18-cm radius circle with the plasma at the center at angles of 6°, 26°, 46°, 66°, and 86° with respect to the normal of the target surface. Each energy monitor contains a BEUV-sensitive silicon photodiode, a thin zirconium foil to reject visible light, and a La/B_4C multilayer mirror with reflectivity centered at about 6.74 nm with a bandwidth of 0.08-nm FWHM [Fig. 1(b)]. The total (foil, mirror, and photodiode) spectral responsivity of each energy monitor is calibrated using the Advanced Light Source (ALS) synchrotron [Fig. 1(c)]. The measurement of the BEUV emission from near-normal to near-grazing incidence with calibrated detectors allows for accurate conversion-efficiency measurements. The spectral emission is measured using a flat-field grazing incidence spectrometer consisting of a variable-line-spacing diffraction grating with a nominal ruling of 1200 lines/mm and a back-illuminated CCD detector. The spectrometer, which has a spectral resolution of about 0.03 nm, is calibrated using the second diffraction order of C V/ C VI emission lines which are excited by irradiating a graphite target. The spectrometer is placed to observe the spectral emission at angles of 20°, 60°, and 85° with respect to target normal. The efficiencies of the spectrometer diffraction grating and foil filter over the spectral band of interest are also calibrated at the ALS.

In addition, we use a BEUV imaging system to measure the size of the BEUV-emitting plasma region from both the normal (front view) and lateral (side view) direction. Images of the plasma emission at BEUV wavelength are obtained using a La/B_4C multilayer concave mirror with a radius of curvature of 230 mm and a EUV-sensitive CCD. The magnification of this imaging system for front-view imaging and side-view imaging is 13× and 14×, respectively. The combination of the La/B_4C multilayer mirror with Ag and Al foils to block longer wavelength light ensures that only the emission near $\lambda = 6.7$ nm contributes to the plasma images. The characteristics of this imaging system include high in-band fluence that results in a high signal-to-noise ratio and a spatial resolution of ~5 μm on the object plane limited by a spherical aberration of the mirror. Since the size of the plasmas in our experiments is in the range from 30 to 100 μm, this imaging system has the capability of producing high resolution in-band images of the plasma sources

III. SPECTRAL CHARACTERIZATION

In this section we discuss the spectral characterization of the Gd and Tb plasmas. This includes the variations of the BEUV spectral emission as a function of laser-pulse duration, viewing angle, and spatial location within plasma. To measure the BEUV spectral emission as function of laser-pulse duration the spectrometer is aligned to capture the plasma emission at an angle of 60° from the target normal. The plasmas are produced by laser pulses with a focal spot size of 55 μm, pulse energy of 60 mJ, and different pulse durations between 120 ps and 4 ns corresponding to intensities between 4.1×10^{11} and 1.4×10^{13} W cm^{-2}. As shown in Fig. 2(a), the peak emission wavelength of plasmas created with 120 and 220 ps pulses is measured to be around 6.93 nm, and that for the 2-ns and 4-ns pulses is measured to be near 6.78 nm. A shift in the peak emission is also observed when we increased the laser-pulse energy from 20 to 80 mJ while keeping the laser-pulse duration and focal spot size constant. Spectra of the emission from Tb plasmas acquired under the same laser-irradiation conditions are shown in Fig. 2(b). They demonstrate a similar trend to that observed for the Gd-plasma emission, with plasmas generated by shorter pulses emitting at longer wavelengths. The wavelength of the Tb plasma emission is shorter than that of the Gd-plasma emission: the peak wavelength of the spectrum from plasmas produced by the same laser-pulse durations is

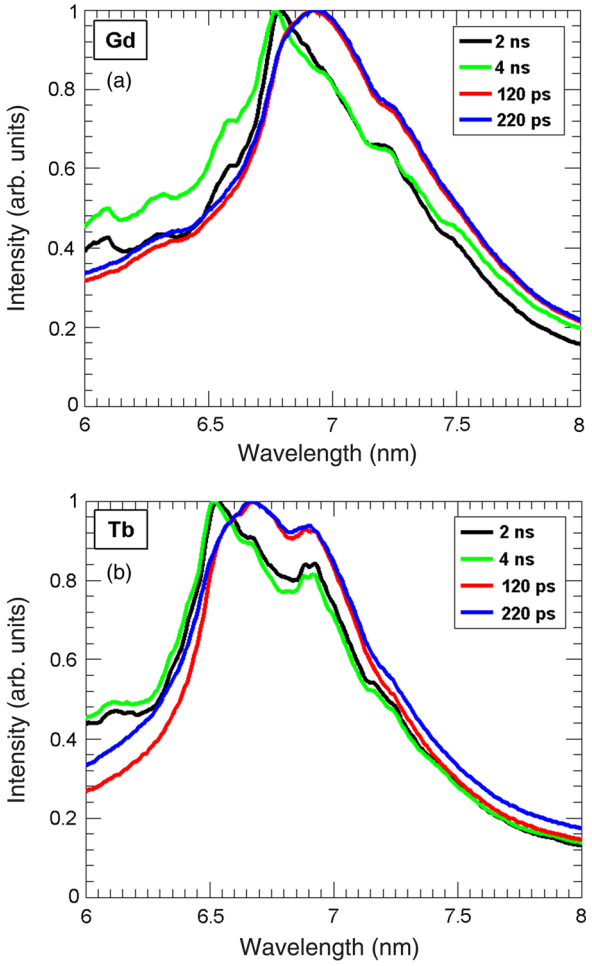

FIG. 2. Measured Gd (a) and Tb (b) spectra corresponding to plasmas generated by 60-mJ pulses with different pulse durations. The laser-focus spot size on target is 55 μm. The spectra are measured at 60° from the target normal.

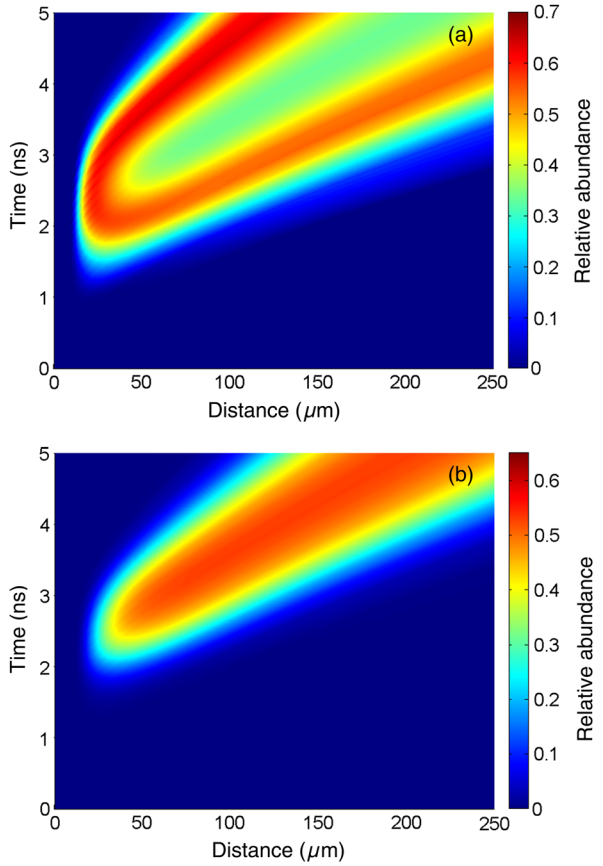

FIG. 3. A simulation of the relative ion abundance of: (a) Rh-like Gd^{19+}; (b) Ru-like Gd^{20} for a Gd plasma created with a 60-mJ pulse of 2-ns duration spot 55-μm FWHM spot size. The horizontal axis represents the distance from the target surface and the vertical axis represents the time from the beginning of the laser pulse.

measured to be near 6.67 nm for the plasmas created with the picosecond pulses, and 6.52 nm for nanosecond pulses respectively.

As noticed above, the peak emission shifts to longer wavelength as the laser-pulse duration is shortened. This wavelength shift is caused by the increase of the mean ion charge that occurs when the pulse duration becomes shorter and the irradiation intensity increases. The model simulation results shown in Figs. 3(a) and 3(b) indicate that the dominant ions in the Gd plasmas created using 2-ns laser pulses are Rh-like Gd^{19+} and Ru-like Gd^{20+} and Figs. 4(a) and 4(b) show the simulated temperature of the plasma created with 2-ns and 220-ps laser pulses, respectively. The laser-pulse energy is 60 mJ and laser spot size is 55 μm for both pulse durations for the simulation. The plasma created by the 2-ns laser pulses is computed to have a maximum electron temperature of ~110 eV, while the plasma created by 220-ps laser pulses has a maximum temperature of ~300 eV. The higher plasma temperature in the latter case causes an increase in the ion charge state Z. Since the mean wavelength of the $n = 4$–4 transitions in Gd ions ($Z > 18+$) shifts to a longer wavelength as the ion charge increases [4,27], the spectral emission of Gd plasmas created using picosecond laser-pulse shifts accordingly with respect to the emission of Gd plasmas created using nanosecond laser pulses. This somewhat-unusual effect of decreased photon energy with increased Z is due to the increased splitting of a $n = 4$ ground state when the Gd ion is ionized from the closed shell Pd-like ionization state to higher ionization states according to our simulation. The spectra obtained with the picosecond laser-pulse durations are also observed to be broader than those obtained with the nanosecond laser pulses. Two different facts contribute to this effect. First, the hotter picosecond plasma has a broader distribution of ion species, which in combination emit over a broader bandwidth. Second, as these $4d$ ions become more highly ionized ($Z > 18+$) the transitions $4p^6 4d^m$-$(4p^5 4d^{m+1} + 4p^6 4d^{m-1} 4f)$ emit over a broader spectral range. The broadening and spectral shift of the Tb plasma to longer wavelengths for shorter laser pulses

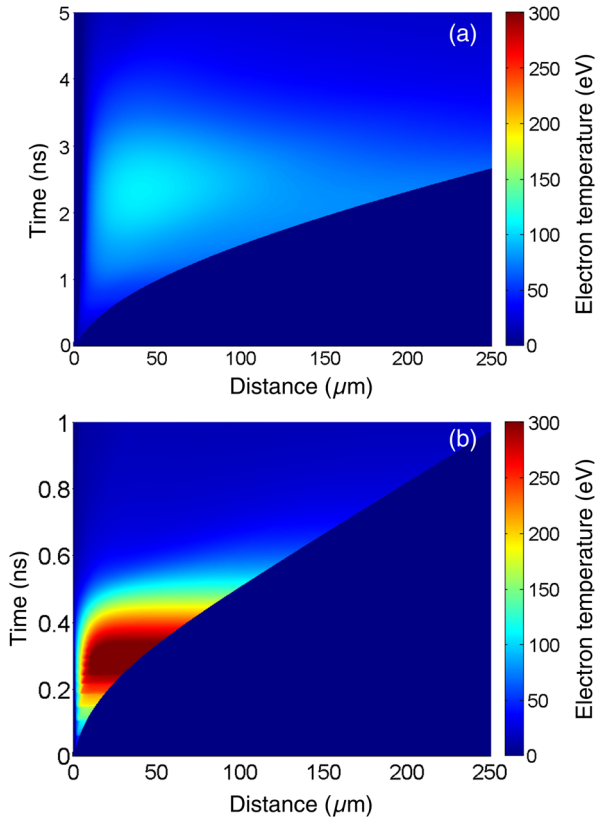

FIG. 4. Simulated plasma temperature (eV) for plasmas created by 2-ns (a) and 220-ps (b) laser pulses. The laser-pulse energy is 60 mJ and the focus spot size is 55 μm.

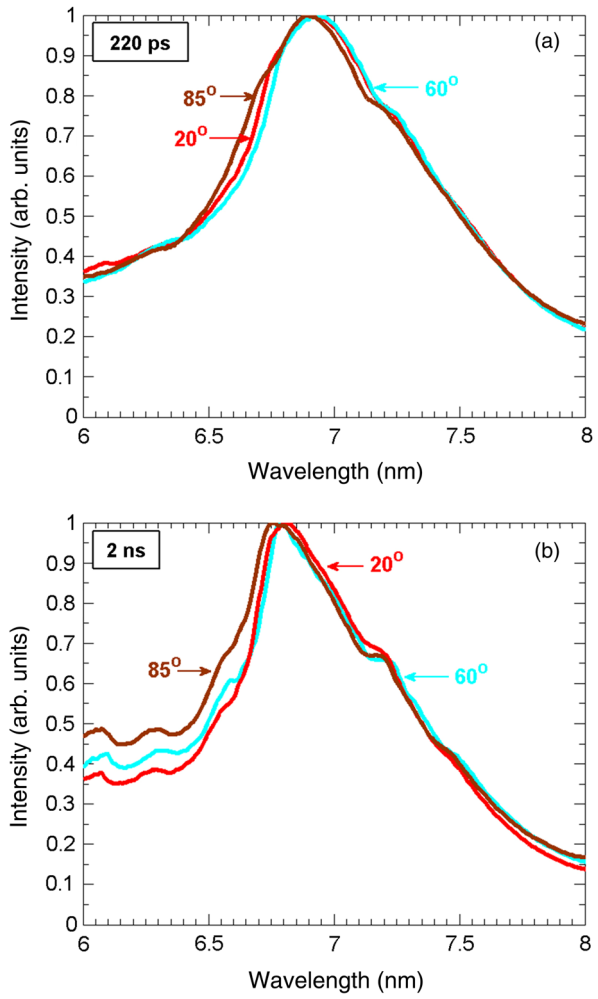

FIG. 5. Measured spectral emission of the Gd plasmas at observation angles of 85° (brown), 60° (cyan), and 20° (red) from the target normal for three pulse durations 220 ps (a), 2 ns (b). The pulse energy is 60 mJ and the focal spot size is 55 μm.

[Fig. 2(b)] is due to the same physics that causes the similar phenomena observed in Gd.

BEUV spectral emission is also measured at angles of 20° and 85° from the target normal for two laser-pulse durations of 220 ps, 2 ns to study the angular dependence of the BEUV spectral emission. A laser-pulse energy 60 mJ and focal spot size of 55 μm are also employed for these measurements. The spectral emission from these plasmas is similar for all angles as shown in Figs. 5(a) and 5(b).

The above spectroscopic studies correspond to the emission from the entire Gd plasma. In order to better understand the origin of the emission, a 20 -μm slit is used to define the plasma region from which the spectrometer gathers the light. The slit is placed about 3 mm away from the plasma and is mounted on a motorized stage. The plasma is created by focusing 220-ps, 60-mJ driver laser pulses into a 55 -μm spot on a Gd planar target. The slit is moved in 20 -μm steps along the direction normal to the target surface to allow the emission from a 20 -μm slice of Gd plasma to be recorded by the spectrometer on each step. The results are shown in Fig. 6. In order to verify the validity of the measurement, we sum the spectra corresponding to all plasma regions to form a whole-plasma spectrum and compare it with the 220-ps spectra in Fig. 2(a) acquired without the slit. The two spectra match very well.

As seen in Fig. 6(a), as the distance from the target surface increases, the spectral emission initially becomes stronger and peaks at about 50 μm from the surface. At larger distances, the spectral emission becomes weaker. In Fig. 6(b) the spectra corresponding to each plasma location are normalized to allow for a better comparison of the spectral distributions. The spectral width becomes narrower as the distance increases. As the slit is moved from 50 to 150 μm, the peak of the spectrum also shifts towards shorter wavelengths from 6.98 to 6.80 nm. This occurs because as the slit is placed to collect light from distances far from the target the contribution to the emission originates from the lower charge ions. The $n = 4$–4 transitions of Pd-like Gd^{18+} ions and the $n = 5$–1 transitions of lower charge ions contribute to the shift towards lower wavelengths. In contrast, from 50 to 150 μm the shift of the peak of the spectrum for plasma produced with 4-ns laser pulse is much smaller, as demonstrated in Fig. 6(c). Figures 6(b) and 6(c) show that the plasmas produced with

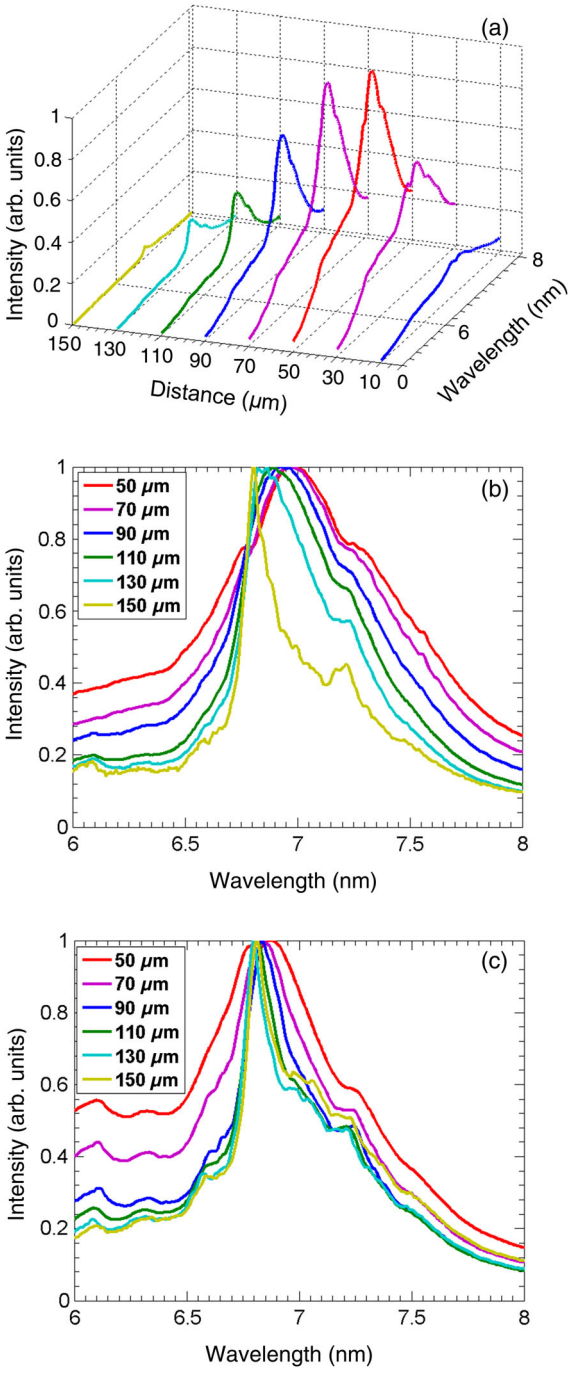

FIG. 6 (a) Spectral emission of the Gd plasma produced with 220-ps laser pulse at different distances from the target surface. (b) Normalized spectral emission of the Gd plasma produced with 220-ps laser pulse at different distances from the target surface. (c) Normalized spectral emission of the Gd plasma produced with 4-ns laser pulse at different distances from the target surface. The plasmas are created by focusing 220 ps/4 ns, 60-mJ pulses into a 55-μm spot.

the picosecond pulses have a significantly larger spectral shift of the BEUV emission as a function of distance from the target, as compared with the plasmas generated by the nanosecond pulses, broadening the spectra.

Figure 7(a) shows the spatial distribution of the spectral emission from a Gd plasma produced with a 220-ps laser pulse. The spatial distribution of the spectral emission is formed by stacking the spectra obtained at different distances along the target normal. The spatial-intensity profile of the emission near $\lambda = 6.74$ nm, which is obtained by spectrally integrating the emission falling in the reflectivity band of the La/B_4C mirror used for plasma imaging in Sec. VI, is shown in Fig. 7(b). The intensity peak of the Gd-plasma emission is observed to occur at 50 μm from the target surface. This measured spatial-intensity profile matches that obtained from plasma imaging under the same laser condition discussed in Sec. VI. The good agreement between the integral of the measured spatial distribution of the spectral emission and the spatial distribution of the source intensity obtained from imaging the plasma under the same laser conditions [Fig. 7(b)] helps to validate the measurements.

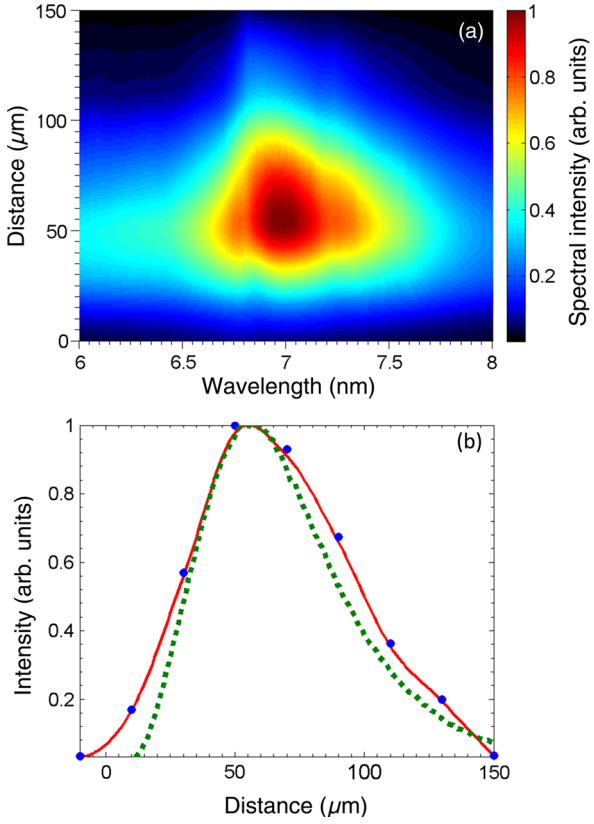

FIG. 7. (a) Spatially resolved spectral profile of Gd plasma produced with 220-ps laser pulse formed by combining the spectra shown in Fig. 6(a). Cubic interpolation between spatial steps is used to smooth the profile. (b) The spatial-intensity profile of the emission near $\lambda = 6.7$ nm obtained from (a). Original data shown as blue solid dots, and interpolation shown as a red solid line compared with the spatial-intensity profile of Gd-plasma emission near $\lambda = 6.7$ nm obtained from the plasma image in Sec. VI obtained (green dashed line) for the same laser-irradiation conditions.

IV. ANGULAR DISTRIBUTION OF THE BEUV EMISSION

The angular distribution of the BEUV emission shown in Fig. 8 is obtained using an array of energy monitors covering one entire quadrant. The total BEUV yield is obtained by fitting the measured data with a second-order polynomial and integrating this angular distribution of the emission over a solid angle of 2π. The Gd-plasma emission is assumed to be symmetric about the central axis of the plasma. Irradiation parameters including the pulse duration, pulse energy, and focal spot size are scanned when measuring the angular distribution of the BEUV emission. This allowed us to investigate how the irradiation parameters influence the angular distribution of the emission and to more precisely determine the conversion efficiency by integrating the real angular distribution of the emission over 2π instead of assuming an isotropic distribution as done in previous measurements [11,13]. Figure 8(a) shows a comparison of the angular distributions of emission for different laser-pulse durations while the 60-mJ laser-pulse energy and 55 μm focal-spot diameter remain constant. In Fig. 8(b) each angular intensity distribution is normalized to the same maximum to facilitate the comparison of the shape of the angular distribution. The first observation is that the emission decreases as the angle with respect to the target normal increases, which is also observed for Tin laser-produced plasmas [28]. Also the angular distribution of the emission corresponding to the shorter pulse duration is more convex. This is possibly the result for the dynamic Doppler effect being more prominent in the hotter plasmas of the picosecond pulses, which shifts the emitting line frequencies due to velocity gradients in the accelerated plasma. This makes the resonant absorption lines more transparent in the direction normal to the target than parallel to the target surface. The average influence of this effect is small, as it affects only the strongest resonance lines while the majority of other 4-4 lines remain close to being optical thin. In addition, a comparison of the angular distributions for focal spots of 30-μm FWHM and 55-μm FWHM shows that the focal spot size does not greatly affect the angular distribution of the emission.

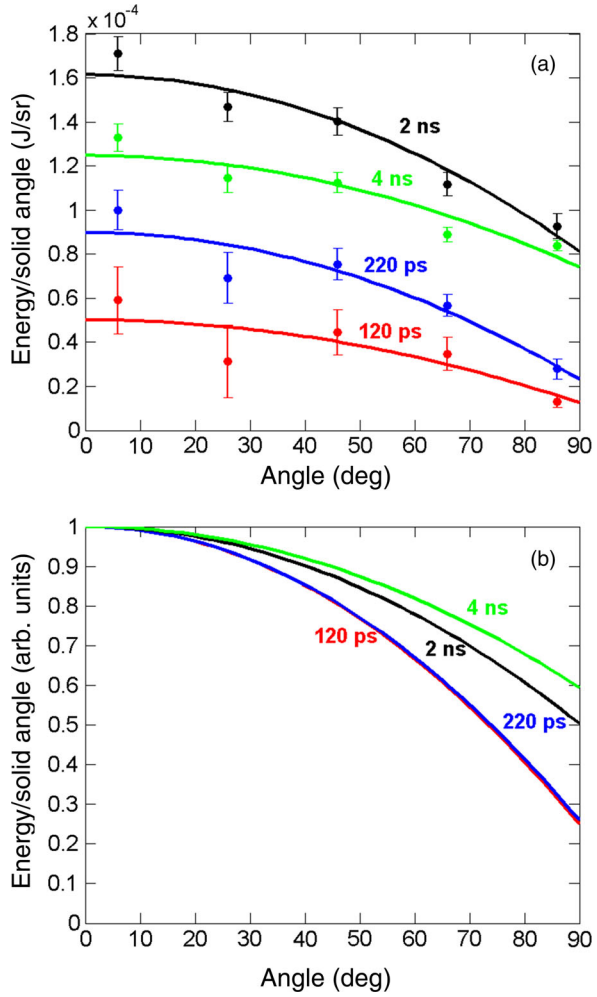

FIG. 8. (a) Measured angular distributions of the BEUV emission from Gd plasmas created with laser-pulse durations of 120-ps FWHM (red), 220-ps FWHM (blue), 2-ns FWHM (black), and 4-ns FWHM (green) while the laser-pulse energy remained 60 mJ and the focal spot size remained 55-μm FWHM. The curves are second-order polynomial fits to the data; (b) fits of the data from (a) normalized for the purpose of comparison of the angular distribution corresponding to different pulse duration.

V. CONVERSION-EFFICIENCY MEASUREMENTS

Figure 9 shows the measured CE of laser-pulse energy into $\lambda = 6.7$ nm emission energy for both Gd [Fig. 9(a)] and Tb [Fig. 9(b)] plasmas for different laser intensities ranging from 1.4×10^{11} W/cm^2 to 6.1×10^{13} W/cm^2. Each curve is obtained by varying the laser-pulse energy while keeping all other parameters constant. The highest CE for Gd, 0.47%, is obtained at a laser intensity of 6.8×10^{11} W/cm^2 with a laser-pulse duration of 2 ns. Both the maximum CE value and the laser intensity at which the maximum CE occurs are similar to those reported in previous modeling work [29]. It should be noticed that if the CE were to be computed using the data from a single detector placed at 45° assuming an isotropic distribution, the CE values would be overestimated by up to 28%. The discrepancy between CE values obtained from measuring the angular distribution and assuming an isotropic angular distribution increases as the laser pulse becomes shorter because in this case the angular distribution of the emission becomes more convex as shown in Fig. 8. As shown in Fig. 4, the Gd plasmas created using the 220-ps laser pulses are much hotter than those created with the 2-ns laser pulse, which causes the spectral emission of the Gd plasma to shift to more highly ionized species and away from the peak of responsivity of the energy monitors. As discussed in Sec. III the spectra of the Gd plasmas

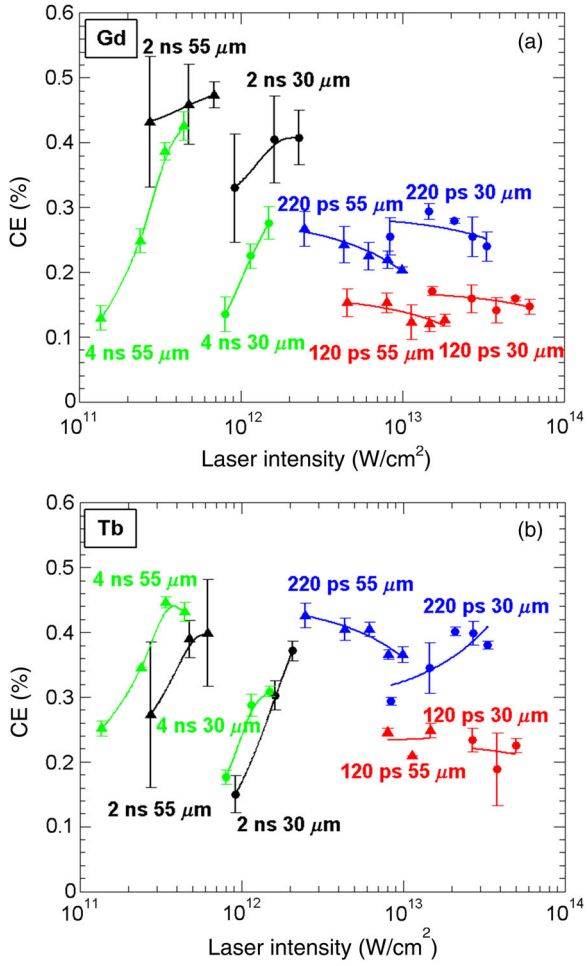

FIG. 9. Measured dependence of CE on laser intensity for (a) Gd and (b) Tb plasmas. The CE is measured for four pulse durations: 120-ps FWHM (red), 220-ps FWHM (blue), 2-ns FWHM (black), and 4-ns FWHM (green) for two different spot sizes: 30-μm FWHM (solid dots) and 55-μm FWHM (solid triangles) as a function of laser-pulse energy. For each condition (pulse duration, pulse energy, focal spot size), the mean of 5 shots is shown. The BEUV emission energy for each shot is computed by integrating the angular distribution over a 2π solid angle.

created using 2- and 4-ns duration pulses overlap better with the responsivity of the energy monitors used in the CE measurements. Additionally, in the nanosecond regime the observed CE corresponding to the case of laser focal spot size of 55 -μm FWHM is higher than that with focal spot size of 30 -μm FWHM, which is predicted by modeling work [30]. This is because the smaller plasma created by the latter cools faster due to the larger expansion heat loss [10], making the ratio of the radiative lifetime-to-hydrodynamic cooling time larger.

The measured dependence of the CE of the Tb plasma on laser intensity is similar to that of the Gd plasma, except that the CE of the Tb plasma for the picosecond laser pulse is higher than the CE of the Gd plasma created with the same laser-pulse duration. The reason for this is that in the case of the picosecond laser pulse the spectral emission of the Tb plasma has a better overlap with the responsivity of the energy monitors than that of the Gd-plasma emission. The best CE for the Tb plasma is measured to be 0.45% which is obtained with a driver laser intensity of 3.4×10^{11} W/cm^2. These results indicate that the precise responsivity of the BEUV energy monitors plays a significant role in the measured conversion efficiency and must be taken into account when comparing the results between different experiments.

VI. PLASMA IMAGING

Plasma imaging allows us to determine the size of the BEUV-emitting plasma region and the pattern of the

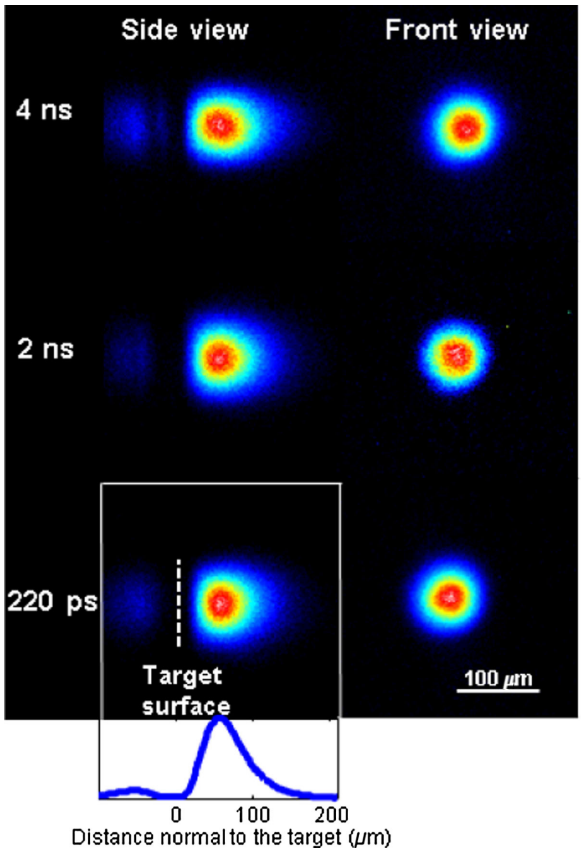

FIG. 10. Plasma images of the BEUV-emitting region from Gd plasmas obtained focusing 60-mJ laser pulses into a spot diameter of ~55 μm (FWHM). The left column shows side-view plasma images viewed parallel to the target surface. The images in the right column are front-view plasma images taken in the direction normal to the target surface. Side-view and front-view plasma images corresponding to 220-ps, 2-ns, and 4-ns FWHM laser-pulse durations are shown. Each plasma image is normalized to its maximum intensity. The inset plot shows the position of the target surface (dashed line) determined by dividing the distance between the maxima of the plasma emission and its reflection from the target surface. The inset also shows the intensity profile of the side-view image.

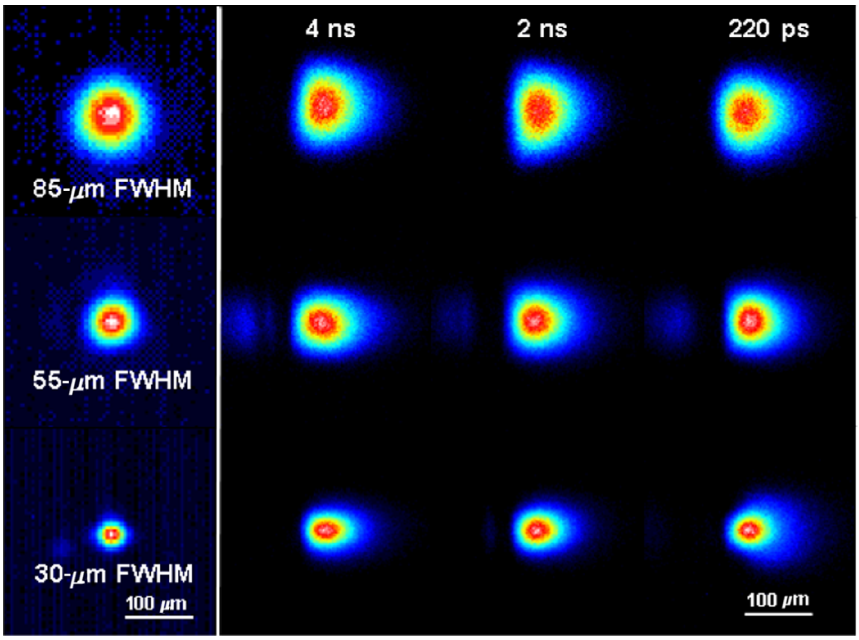

FIG. 11. Side-view plasma images corresponding to different laser-focus spot sizes and pulse durations. The laser is focused into spots with diameters of ~85, ~55, and ~30 μm (FWHM). The first column shows the laser spot focus on target. Each row on the right shows side-view plasma images taken with laser-pulse durations of 4-ns, 2-ns, and 220-ps FWHM (left to right). The pulse energy is 60 mJ for all images. Each image is normalized to its maximum intensity.

Gd-plasma expansion under different irradiation conditions. Front-view and side-view images of the Gd plasmas at the BEUV wavelength are obtained for different laser-focus spot sizes and pulse durations. With a laser-pulse energy of 60 mJ, a focal spot size of 55 -μm FWHM, and laser-pulse durations varying from 220 ps to 4 ns, we obtained the front-view and side-view images as shown in Fig. 10. The BEUV-emitting region of the Gd plasmas has a lateral dimension (parallel to target surface) similar to the laser spot size and is insensitive to the laser-pulse duration. The side-view Gd-plasma images in Fig. 11 are taken for laser-focus spot sizes of 30, 55 and 85 μm. For each laser-focus spot size the laser-pulse duration is varied, while the pulse energy remains at 60 mJ. As the size of the laser focus decreases, the plasma size in the lateral direction decreases and the lateral expansion of the plasma becomes stronger. In the direction normal to target, the size of the BEUV-emitting plasma shrinks slightly as the laser focal spot size decreases. The side-view images show the reflection of the Gd-plasma emission from the target surface, as seen in Fig. 10. We determine the location of the target surface using the reflected BEUV light from the target surface. The peak of the BEUV-emitting plasma region is measured to be located about 50 μm from the surface of target and is rather insensitive to the laser-pulse duration. Fig. 12 shows a simulated BEUV emission density map for a Gd plasma created focusing a 2 ns, 60 mJ laser pulse into a 55 μm diameter spot. In the simulated emission density map we can see the BEUV emission peak is also located about 50 μm from the target and the size of the BEUV-emitting plasma region in the normal direction is about 85 -μm FWHM, which matches well with the experimental image taken under the same laser conditions.

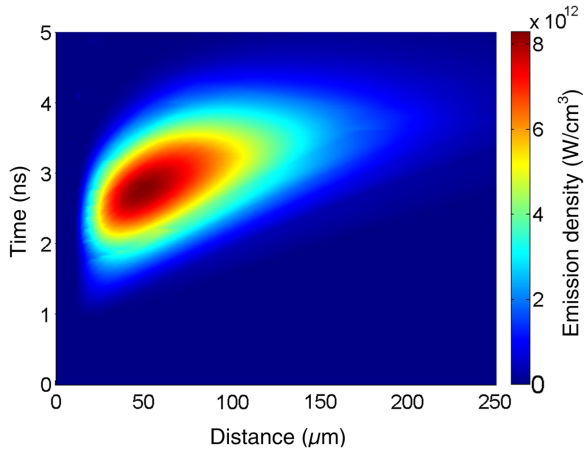

FIG. 12. Simulated spatial-temporal distribution of the BEUV emission density (W/cm^3) of a Gd plasma created by focusing a 2-ns, 60-mJ laser pulse into a 55-μm FWHM spot.

VII. SUMMARY

In conclusion, we conduct a comprehensive study of the emission of laser-produced Gd and Tb plasmas at wavelengths near 6.7 nm with both experiments and simulations. The measurements are conducted by focusing laser pulses of durations ranging from 120 ps to 4 ns from a single $\lambda = 1030$ nm laser onto a slab target. We measure the spectral emission, the angular distribution of the emission, the conversion efficiency, and the plasma source size for different irradiation conditions. All the measurements are conducted over a broad range of parameters using a single laser and the same setup, which allows for increased consistency. Model simulations conducted with a transient hydrodynamic and atomic physics model with radiation

transport show that in the Gd plasmas created at an irradiation intensity of 8.2×10^{11} W cm^{-2} using 2-ns laser pulses, the dominant ions are Rh-like Gd^{19+} and Ru-like Gd^{20+}. The spectral measurements show that the wavelength of the peak spectral emission shifts from 6.78 nm to a longer wavelength and the spectrum becomes broader when the laser-pulse duration is reduced from 2–4 ns to 120–220 ps. The associated increase in irradiation intensity causes the plasma emission to originate from more highly ionized species whose transitions are increasingly mismatched with the responsivity of the energy monitor centered at 6.74 nm, causing a decrease in the amount of BEUV emission collected by the energy monitors.

The measurements show that the BEUV emission from Gd plasma is not isotropic. The BEUV emission is measured to decrease as a function of angle from the target normal with the angular distribution of BEUV emission becoming more convex when pulse duration decreases from nanoseconds to hundreds of picoseconds. The conversion efficiency for different irradiation conditions is determined by integrating the measured angular distribution of the BEUV emission. The highest conversion efficiency of 0.47% is obtained for a Gd plasma generated with a laser intensity of 6.8×10^{11} W/cm^2 with a pulse duration of 2 ns, and a laser spot size on target of 55-μm FWHM. However, it should be noticed that the optimum laser pulse width for maximum CE significantly depends on the center wavelength of the responsivity of the energy monitors that are used. This is because, given the rather abrupt spectral profile of the BEUV emission, the laser pulse-width-dependent overlap between the BEUV emission band and the responsivity of the energy monitors can be a dominant effect in determining CE. Therefore, the spectral responsivity of the detectors needs to be taken into account in interpreting CE results and in comparing different results reported in the literature. A similar maximum conversion efficiency of 0.45% is measured for the Tb plasmas irradiated under similar conditions. The measurement of the plasma emission conducted using a diode array indicates that if the CE would have been estimated using a single diode and assuming an isotropic distribution, its value would have been overestimated by up to 28%. The results illustrate the importance of performing angularly resolved measurements of the plasma emission to compute CE. For a smaller laser spot size, the lateral expansion of the plasma is stronger, resulting in faster cooling and lower conversion efficiency. The size of the BEUV-emitting region is measured to be very similar to the laser spot size and the peak of the BEUV-emitting plasma region is found to take place at a distance of about 50 μm from the target surface, in agreement with simulations. The measured CE does not represent the maximum that can be obtained near this wavelength. Our atomic physics calculations estimate that a CE of up to 6% may ultimately be obtainable in an ideally tailored plasma. Temporal pulse shaping with the inclusion of prepulses and more sophisticated target designs will be required for this purpose.

ACKNOWLEDGMENTS

This work was supported by NSF PFI: AIR, Award No. NSF IIP-1343456, and Cymer LLC. M. B. acknowledges the support of Oak Ridge National Laboratory/DOE. This manuscript has been authored by UT-Battelle, LLC under Contract No. DE-AC05-00OR22725 with the U.S. Department of Energy. The Department of Energy will provide public access to these results of federally sponsored research in accordance with the DOE Public Access Plan. We are thankful to Michael Purvis for helpful discussions and comments.

[1] *Understanding Moore's Law: Four Decades of Innovation*, edited by David C. Brock and Gordon E. Moore (Chemical Heritage Foundation, Philadelphia, PA, 2006).

[2] S. Wurm, EUV lithography: progress, challenges, and outlook, in *30th European Mask and Lithography Conference, 923103*, edited by U. F. W. Behringer, SPIE Proceedings Vol. 9231 (SPIE-International Society for Optical Engineering, Bellingham, WA, 2014).

[3] Alberto Pirati, Alberto Pirati, Rudy Peeters, Daniel Smith, Sjoerd Lok, Arthur Minnaert, Martijn van Noordenburg, Jörg Mallmann, Noreen Harned, Judon Stoeldraijer, Christian Wagner, Carmen Zoldesi, Eelco van Setten, Jo Finders, Koen de Peuter, Chris de Ruijter, Milos Popadic, Roger Huang, Martin Lin, Frank Chuang *et al.*, *Performance overview and outlook of EUV lithography systems, in Extreme Ultraviolet (EUV) Lithography VI, 94221P*, edited by O. R. Wood and E. M. Panning, SPIE Proceedings Vol. 9422 (SPIE-International Society for Optical Engineering, Bellingham, WA, 2015).

[4] S. S. Churilov, R. R. Kildiyarova, A. N. Ryabtsev, and S. V. Sadovsky, EUV spectra of Gd, and Tb ions excited in laser-produced, and vacuum spark plasmas, Phys. Scr. **80**, 045303 (2009).

[5] D. Kilbane and G. O'Sullivan, Extreme ultraviolet emission spectra of Gd and Tb ions, J. Appl. Phys. **108**, 104905 (2010).

[6] Nassir Mojarad, Jens Gobrecht, and Yasin Ekinci, Beyond EUV lithography: A comparative study of efficient photoresists' performance, Sci. Rep. **5**, 9235 (2015).

[7] I. A. Makhotkin, E. Zoethout, E. Louis, A. M. Yakunin, S. Muellender, and F. Bijkerk, Wavelength selection for multilayer coatings for lithography generation beyond extreme ultraviolet, J. Micro/Nanolithogr. MEMS MOEMS **11**, 040501 (2012).

[8] D. S. Kuznetsov, A. E. Yakshin, J. M. Sturm, R. W. E. van de Kruijs, E. Louis, and F. Bijkerk, High-reflectance La/B-based multilayer mirror for 6.x nm wavelength, Opt. Lett. **40**, 3778 (2015).

[9] Hayato Ohashi, Takeshi Higashiguchi, Bowen Li, Yuhei Suzuki, Mashato Kawasaki, Tatsuhiko Kanehara, Yuya Aida, Shuichi Torii, Tetsuya Makimura, Weihua Jiang,

Padraig Dunne, Gerry O'Sullivan, and Nobuyuki Nakamura, Tuning extreme ultraviolet emission for optimum coupling with multilayer mirrors for future lithography through control of ionic charge states, J. Appl. Phys. **115**, 033302 (2014).

[10] G. J. Pert and S. A. Ramsden, Population inversion in plasmas produced by picosecond laser pulses, Opt. Commun. **11**, 270 (1974).

[11] Thomas Cummins, Takamitsu Otsuka, Noboru Yugami, Weihua Jiang, Akira Endo, Bowen Li, Colm O'Gorman, Padraig Dunne, Emma Sokell, Gerry O'Sulliva, and Takeshi Higashiguchi, Optimizing conversion efficiency and reducing ion energy in a laser-produced plasma, Appl. Phys. Lett. **100**, 061118 (2012).

[12] Takeshi Higashiguchi, Takamitsu Otsuka, Noboru Yugami, Weihua Jiang, Akira Endo, Bowen Li, Deirdre Kilbane, Padraig Dunne, and Gerry O'Sullivan, Extreme ultraviolet source at 6.7 nm based on a low-density plasma, Appl. Phys. Lett. **99**, 191502 (2011).

[13] Kensuke Yoshida, Shinsuke Fujioka, Takeshi Higashiguchi, Teruyuki Ugomori, Nozomi Tanaka, Hayato Ohashi, Masato Kawasaki, Yuhei Suzuki, Chihiro Suzuki, Kentaro Tomita, Ryoichi Hirose, Takeo Ejima, Masaharu Nishikino, Atsuhi Sunahara, Enda Scally, Bowen Li, Tatsuya Yanagida, Hiroaki Nishimura, Hiroshi Azechi, and Gerry O'Sullivan, Efficient extreme ultraviolet emission from one-dimensional spherical plasmas produced by multiple lasers, Appl. Phys. Express **7**, 086202 (2014).

[14] Takeshi Higashiguchi, Bowen Li, Yuhei Suzuki, Masato Kawasaki, Hayato Ohashi, Shuichi Torii, Daisuke Nakamura, Akihiko Takahashi, Tatsuo Okada, Weihua Jiang, Taisuke Miura, Akira Endo, Padraig Dunne, Gerry O'Sullivan, and Tetsuya Makimura, Characteristics of extreme ultraviolet emission from mid-infrared laser-produced rare-earth Gd plasmas, Opt. Express **21**, 31837 (2013).

[15] Colm O'Gorman, Takamitsu Otsuka, Noboru Yugami, Weihua Jiang, Akira Endo, Bowen Li, Thomas Cummins, Padraig Dunne, Emma Sokell, Gerry O'Sullivan, and Takeshi Higashiguchi, The effect of viewing angle on the spectral behavior of a Gd plasma source near 6.7 nm, Appl. Phys. Lett. **100**, 141108 (2012).

[16] A. V. Vinogradov and V. N. Shlyaptsev, Amplification of ultraviolet radiation in a laser plasma, Sov. J. Quantum Electron. **13**, 1511 (1983).

[17] Yu. V. Afanas'ev, V. P. Avtonomov, N. G. Basov, G. Korn, G. V. Sklizkov, and V. N. Shlyaptsev, Radiative transport in a laser plasma, J. Russ. Laser Res. **10**, 1 (1989).

[18] M. C. Marconi, C. H. Moreno, J. J. Rocca, V. N. Shlyaptsev, and A. L. Osterheld, Dynamics of a microcapillary discharge plasma using a soft x-ray laser backlighter, Phys. Rev. E **62**, 7209 (2000).

[19] M. Berrill, Y. Wang, M. A. Larotonda, B. M. Luther, V. N. Shlyaptsev, and J. J. Rocca, Pump pulsewidth dependence of grazing incidence pumped transient collisional soft x-ray lasers, Phys. Rev. A **75**, 063821 (2007).

[20] A. V. Vinogradov and V. N. Shlyaptsev, Characteristics of a laser plasma x-ray source (review), Sov. J. Quantum Electron. **17**, 1 (1987).

[21] R. F. Smith, J. Dunn, J. Nilsen, V. N. Shlyaptsev, S. Moon, J. Filevich, J. J. Rocca, M. C. Marconi, J. R. Hunter, and T. W. Barbee, Jr., Picosecond X-ray Laser Interferometry of Dense Plasmas, Phys. Rev. Lett. **89**, 065004 (2002).

[22] M. Klapisch, M. Busquet, and A. Bar-Shalom, A new and improved version of HULLAC, AIP Conf. Proc. **926**, 206 (2007).

[23] A. H. Curtis, B. A. Reagan, K. A. Wernsing, F. J. Furch, B. M. Luther, and J. J. Rocca, Demonstration of a compact 100 Hz, 0.1 J,diode-pumped picosecond laser, Opt. Lett. **36**, 2164 (2011).

[24] Brendan A. Reagan, Alden H. Curtis, Keith A. Wernsing, Federico J. Furch, Bradley M. Luther, and Jorge J. Rocca, Development of high energy diode-pumped thick-disk Yb:YAG chirped-pulse-amplification lasers, IEEE J. Quantum Electron. **48**, 827 (2012).

[25] B. A. Reagan, C. Baumgarten, K. Wernsing, H. Bravo, M. Woolston, A. Curtis, F. J. Furch, B. Luther, D. Patel, C. Menoni, and J. J. Rocca, 1 joule, 100 Hz repetition rate, picosecond CPA laser for driving high average power soft x-ray lasers, in *CLEO: 2014, OSA Technical Digest (Online)* (Optical Society of America, Washington, DC, 2014), paper SM1 F.4.

[26] Brendan A. Reagan, Keith A. Wernsing, Alden H. Curtis, Federico J. Furch, Bradley M. Luther, Dinesh Patel, Carmen S. Menoni, and Jorge J. Rocca, Demonstration of a 100 Hz repetition rate gain-saturated diode-pumped table-top soft x-ray laser, Opt. Lett. **37**, 3624 (2012).

[27] D. Kilbane and G. O'Sullivan, Ground-state configurations and unresolved transition arrays in extreme ultraviolet spectra of lanthanide ions, Phys. Rev. A **82**, 062504 (2010).

[28] O. Morris, F. O'Reilly, P. Dunne, and P. Hayden, Angular emission and self-absorption studies of a tin laser produced plasma extreme ultraviolet source between 10 and 18 nm, Appl. Phys. Lett. **92**, 231503 (2008).

[29] Majid Masnavi, John Szilagyi, Homaira Parchamy, and Martin C. Richardson, Laser-plasma source parameters for Kr, Gd, and Tb ions at 6.6 nm, Appl. Phys. Lett. **102**, 164102 (2013).

[30] Tatyana Sizyuk and Ahmed Hassanein, Optimizing laser produced plasmas for efficient extreme ultraviolet, and soft x-ray light sources, Phys. Plasmas **21**, 083106 (2014).